

Quantum Control for an Experimental Contactless Energy Transfer System for Multiple Users

Fredrik F. A. Van der Pijl, Pavol Bauer, Jan. A. Ferreira, Henk Polinder

Electrical Power Processing group of the Faculty of Electrical Engineering, Mathematics and Informatics
Technical University of Delft
Delft, The Netherlands
f.vanderpil@ewi.tudelft.nl

Abstract— A new system that uses inductive energy transfer to transport energy from a source to a number of variable loads simultaneously is introduced in this paper. Reported is on the controller implementation, based on quantum conversion and sliding-mode control theory, for the system. For both the source and each of the loads a separate controller is present to meet operational requirements. Special in this design is that all controllers work independently and thus are blinded from each other. Result is a proof-of-principle for the energy flow control of the contactless energy transfer system in a laboratory setup.

Keywords— contactless; energy transfer; inductive coupling; multiple output; power transfer; control; sliding-mode

I. INTRODUCTION

INDUCTIVE contactless energy transfer as a future common technique for use as part of a general energy supply network will only have a chance if the energy transfer will be efficient. Until now, contactless transfer is associated with relative high energy loss compared to transfer with cables and thus is applied only in situations where efficiency is not crucial [1] or where the loads are known [2] and can be anticipated on.

Recently, a new inductive contactless energy transfer system has been introduced, of which operation can be compared to a plug-and-socket extension cable [3]. Instead of inserting a plug into a socket, a connection between supply cable and loads (clamps) in the inductive system is established without making electrical contact. Here, the loads are unknown in number and variable in energy demand.

In [3] the system was tested under static conditions in open-loop dynamics, whereas in this paper active controllers are designed to obtain a closed-loop system.

Contribution of this paper is the application of quantum conversion [4] in a more complex environment of multiple independent loads. Furthermore, sliding-mode theory is applied to implement control. It will appear that the relative loose coupling between supply cable and loads (clamps) adds some interesting aspects in modeling the control system.

Because this type of control in a contactless environment is new, objective is an experimental proof of principle. Good examples of the control method as applied in this paper (in different applications) can be found in [5], [6] and [7].

Chapter II introduces the control problem in the contactless environment. Chapter III discusses the control strategy to solve the problem. Subject of chapter IV is a review on the system efficiency. In chapter V the controller implementation is discussed. Chapter VI summarizes experimental results. Chapter VII concludes the work.

II. CONTROL PROBLEM FOR THE CONTACTLESS SYSTEM

An impression of the contactless system is shown in Fig. 1, with blocks denoting the positions of the converters. Controllers are designed for them to regulate the energy flow in the system. Input source for the system is the utility grid. Each of the clamps outputs 60 Hz, 240 V (European 50 Hz, 240 V).

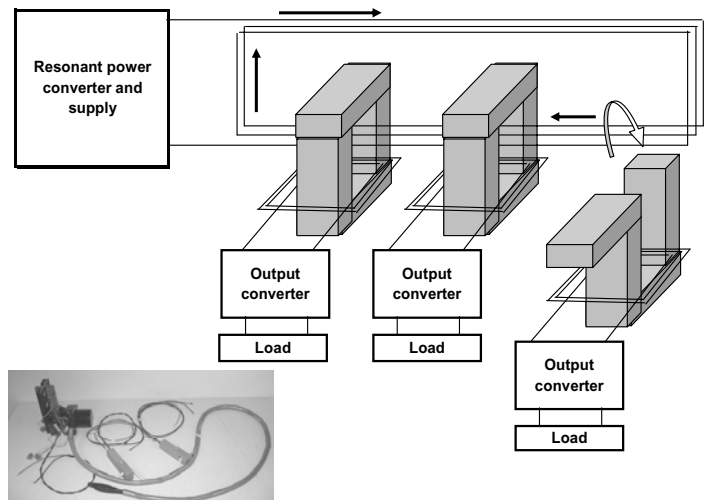


Fig. 1. Contactless system with two clamps attached and one ready to be connected. Arrows next to the conductor spiral denote current direction. At the left bottom the prototype is shown.

In [3] the transformer was designed, resulting in a prototype cable and two clamps with the parameters given in Table 1. An electrical model of the system is shown in Fig. 2. The main electrical current loop (denoted by the arrows) is operated at exactly the resonant frequency of the series L_r - C_r combination, at a (designed) frequency near 80 kHz. This relative high frequency has been chosen to limit the size of the magnetic

cores in the clamps and resonant operation compensates the typical high voltage drop across the leakage inductance L_r . The eight-switch output converter ensures bi-directional energy flow.

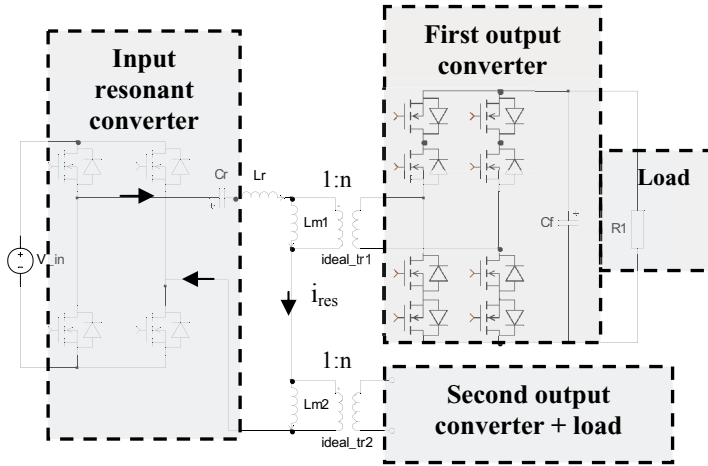


Fig. 2. Electrical model of the contactless system in Fig. 1

TABLE I
PARAMETER VALUES FOR THE CABLE WITH TWO CLAMPS IN THE PROTOTYPE

Symbol	Quantity	Value
C_r	Resonant capacitance	100 nF
L_r	Cable leakage inductance	35.3 [μH]
L_{m1}	Magnetizing inductance of first cable-clamp connection	35.0 [μH]
L_{m2}	Magnetizing inductance of second cable-clamp connection	38.6 [μH]
1:n	Transformer winding ratio (absolute)	1:6 (7:42) [-]

A. Input resonant power converter

The systems' power source is the utility grid. After rectification (V_{in} in Fig. 2), this voltage source must be converted to behave like a high frequent resonant current source for the loads.

Signals behind the magnetizing inductances in Fig. 2 are not available as inputs for the input controller. Also, the number of loads and their individual energy demand are variable.

B. Output clamp converters

All clamps share the same electrical current i_{res} and each output voltage waveform is required to be 50-60 Hz, 240 V. Therefore, the use of an active converter to regulate the power is unavoidable.

III. QUANTUM CONTROL STRATEGY FOR THE CONTACTLESS SYSTEM

A. Quantum conversion

Sliding-mode quantum conversion as a control method for resonant circuits has been treated extensively in for example [5], [6] and [7]. Quantum conversion in essence is a current

pulse based switching method. Switching is done at the resonant frequency and exactly at the zero-crossing of the current through the switches.

Result is a discrete system, in which a half period of the current is the smallest entity (quantum) and thus determines the resolution of the system. For each current quantum it can be decided (by a switching state) to add or subtract its associated energy from the system. Also, a quantum can be short-cut (neglected), which means that the energy in the system is kept equal. For both input converter and output converters this switching principle is used. Fig. 3 shows the principle.

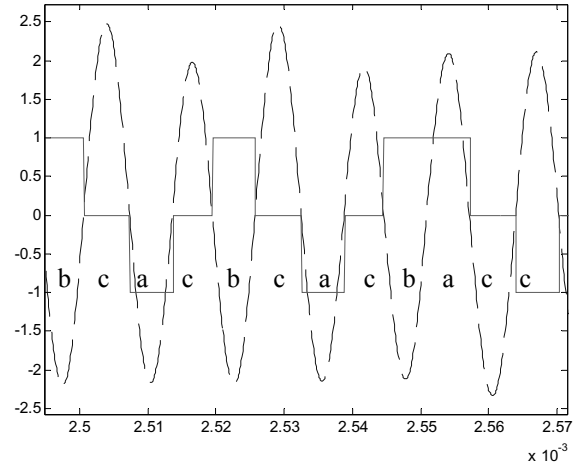


Fig. 3. Quantum conversion, with a) powering, b) regeneration and c) free-resonant modes. The present mode is determined by the product of the solid block signal, denoting the switching signal {1, 0, -1}, and the resonant current (dotted).

B. Sliding-mode control

Sliding-mode control [8], has been applied in [6] to a resonant converter with a comparable topology as in Fig. 2. Significant difference is a magnetizing inductance that is present in Fig. 2, but absent in [6]. The latter inductance is relative small, because of the loose magnetic coupling between clamp and cable.

Sliding-mode theory in general is powerful from the fact that non-linear higher order open-loop system dynamics are combined with controller dynamics (sensed signals) into a linear sliding surface. This surface in essence reduces the control problem to a linear first order problem. Challenge is to find a proper sliding surface, which is the case when it satisfies the three conditions of existence, reaching and invariance.

Sliding-mode theory is now interesting as a control method for the contactless system, because it is possible to make a combination of multiple sliding surfaces. For example, with two independent sliding surfaces, the resulting sliding 'surface' is the intersection of both and thus actually is a sliding line. This fits the contactless case, because here the feedback parameters (resonant current for the input, output voltages for the outputs) are independent from each other. As a remark, another possibility would be to communicate

wirelessly between input and output converters to resolve the independency between input and output. This option is not considered, because of the expected relative long communication delay compared to the high switching frequency.

C. Multiple sliding-surfaces

In [6] starting point is the choice for two sliding surface candidates in (1) and to see if they satisfy the three sliding conditions.

$$S_{input} = I_{ref} - i_{res,av} \quad (1)$$

$$S_{output1} = V_{ref} \sin(\omega t) + v_{o1,av}$$

To have multiple output converters (at least two) a third sliding surface is added in (2).

$$S_{output2} = V_{ref} \sin(\omega t - \alpha) + v_{o2,av} \quad (2)$$

The sliding surfaces are simply the difference between actual variable and required reference value. The arbitrary phase-shift α in (2) is due to the fact that the output controllers are blinded from each other and thus are not synchronized.

If the surfaces (1) and (2) would not meet the sliding conditions, differences between derivatives of the variables and the references could be added. For an approach where a proper sliding surface is synthesized, in contrary to trial and error, is referred to [7].

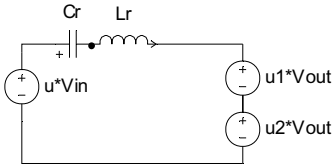


Fig. 4. Simplified model for the contactless system as in Fig. 2 for two clamps, neglecting the magnetizing inductances.

Equations of the system model in Fig. 4 are averaged, resulting in the set of equations (3). Here, the magnetizing inductances are not yet accounted for.

$$\frac{di_{res,av}}{dt} = \frac{V_{in}}{L_{eq}} u - \frac{v_{o1,av}}{L_{eq}} u_{s1} - \frac{v_{o2,av}}{L_{eq}} u_{s2} \quad (3a)$$

$$\frac{dv_{o1,av}}{dt} = \frac{i_{res,av}}{C_0} u_{s1} - \frac{v_{o1,av}}{R_1 C_0} \quad (3b)$$

$$\frac{dv_{o2,av}}{dt} = \frac{i_{res,av}}{C_0} u_{s2} - \frac{v_{o2,av}}{R_2 C_0} \quad (3c)$$

The averaging technique makes use of the discrete nature of quantum converted systems and simplifies the analysis. For details on the method is referred to [9].

Next, the concept of equivalent control [10], where the assumption is to have infinite switching rates, is used to find the parameter boundaries for which the control will be stable.

Assuming sliding regime $S_{input} = 0$, it follows by substitution in (3a) that

$$u_{eq} = \frac{v_{o1,av} u_{s1} + v_{o2,av} u_{s2}}{V_{in}} \quad (4)$$

Inserting (4) in (3b), the intersection of surface $S_{input} = 0$ with $S_{output1} = 0$ gives the equivalent control u_{s1eq} .

$$u_{s1eq} = \frac{1}{R_1 i_{res,av}} \left(v_{o1,av} + R_1 C_0 \frac{dv_{o1,av}}{dt} \right)$$

And accordingly, the equivalent control for the surface $S_{output2} = 0$.

$$u_{s2eq} = \frac{1}{R_2 i_{res,av}} \left(v_{o2,av} + R_2 C_0 \frac{dv_{o2,av}}{dt} \right)$$

Boundaries for the output voltages are now given by the inequalities $-1 < \{u_{s1eq}, u_{s2eq}, \cos(\omega t)\} < 1$.

$$|v_{o1,av}| < R_1 I_{ref} - \omega R_1 C_0 V_{ref} \quad (5a)$$

$$|v_{o2,av}| < R_2 I_{ref} - \omega R_2 C_0 V_{ref} \quad (5b)$$

It is clear from (5) that the output voltage is virtually unlimited by choosing I_{ref} high enough. In this, $\omega [R_1, R_2] C_0 V_{ref}$ is due to the fact that part of the output energy is used to charge and discharge the capacitor C_0 and does not contribute to building up v_{o1} and v_{o2} .

The other way around, starting with the assumptions $S_{output1}, S_{output2} = 0$, it follows that u_{eq} can be written as in (6).

$$u_{eq} = \frac{V_{ref}^2}{V_{in} R_2 R_1 i_{res,av}} \left(R_2 (x_1^2 + \omega R_1 C_0 x_1 y_1) + R_1 (x_2^2 + \omega R_2 C_0 x_2 y_2) \right) \quad (6)$$

where

$$x_1 = \sin(\omega t), x_2 = \sin(\omega t - \alpha),$$

$$y_1 = \cos(\omega t), y_2 = \cos(\omega t - \alpha).$$

Using the inequality $-1 < u_{eq} < 1$ a minimum required (reference) resonant current I_{ref} is found to guarantee stable operation with the given output reference voltage V_{ref} . The minimum depends on the phase shift α and is found by maximizing the right hand side of (6). In the calculation it is assumed that the terms $\omega[R_1, R_2]C_0$ are sufficiently small compared to 1 to be neglected. This can be assured by choosing C_0 small enough. If the resulting ripple on the output voltage will be unacceptable, a penalty must be added to the reference current.

The time at which (6) reaches its minimum [maximum] is given by (7)

$$t_{\max, \min} \left\{ R_2 x_1^2 + R_1 x_2^2 \right\} = \frac{1}{2\omega} \arctan \left(\frac{R_2 \sin(\alpha)}{R_1 + R_2 \cos(\alpha)} \right) \left[+ \frac{\pi}{2} \right] \quad (7)$$

Inserting this time in (6) the minimum required I_{ref} for stable operation is found. Note that the minimum is minimal for $\alpha = \frac{\pi}{2}$, resulting in the smallest conduction loss in the contactless cable. In the unsynchronized contactless prototype the phase α is arbitrary and thus the worst case must be accounted for, resulting in a minimal reference current in (8).

$$I_{ref} > \max \left(\frac{V_{ref}}{R_1}, \frac{V_{ref}}{R_2}, \frac{V_{ref}^2 \cdot (R_1 + R_2)}{V_{in} R_1 R_2} \right) \quad (8)$$

This means that the required output voltage can always be reached, independent of the loads, by choosing the reference value of the resonant current high enough. At the price of a current-penalty it is even possible to have a larger reference output voltage than input voltage. This is not the case for an uncontrolled output converter with diode-bridge.

Note from (8) that the multiple loads for the input appear as parallel. From an efficiency point of view (related to I_{ref}) it is therefore preferable to have a large number of loads.

D. Accounting for the magnetizing inductance

Calculating an average model for the system including (small) magnetizing inductance is a tedious task, because the system order is increased beyond the analytically manageable second order. This can be seen from Fig. 4 in the fact that L_m causes a phase difference between the main resonant current

and the current flowing to $u_1 \cdot V_{out}$. This means that the voltage ‘sources’ V_{in} and V_{out} will not change state synchronous, which is mathematically inconvenient.

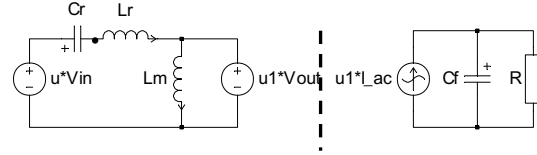


Fig. 5. Model for contactless system with single clamp and including the magnetizing inductance

Important part is that it will be shown next that the latter phase shift can be neglected due to the quantum conversion strategy itself and a modification to it.

E. Strategy to limit the magnetizing current

A solution can be found in realizing that the output voltage is related to the magnetizing inductance by (9).

$$i_{m, k+1} = \frac{1}{L_m} \int_{t=k}^{k+1} u_{s,1,2} \cdot V_{out} \cdot \text{sgn}(i_{res} - i_m) dt + i_{m, k} \quad (9)$$

In (9) the boundaries of integration denote a zero-crossing of the current at time k and the following zero-crossing at $k+1$, with time interval $\frac{1}{2f_{res}}$. The maximum of V_{ref} is known to be the required standard peak grid voltage. Therefore also the maximum increase (or decrease) in i_m in a single half-period (quantum) is known. Result is that with proper quantum switching the magnetizing current amplitude can be kept between two limit values as shown in Fig. 6.

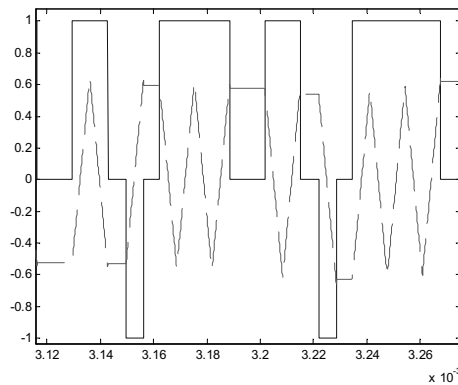


Fig. 6. Demonstration of a switching strategy (solid) to limit the magnetizing inductance (dashed).

A little enhancement of the standard quantum strategy for the output converters is necessary to ensure the current to stay within the limits. In standard quantum conversion the control signal u might change every next quantum. Restricting u to be -1 or 1 results in the problem that a DC component might

appear in the magnetizing current due to consecutive positive integrals in (9), as shown in Fig. 7.

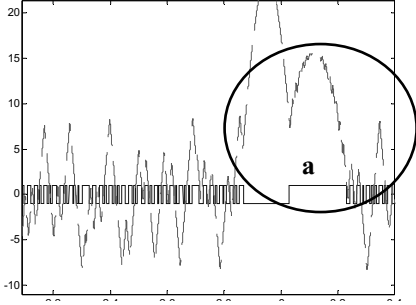


Fig. 7. Matlab Simulink computer simulation of standard asymmetric switching strategy (solid) that results in uncontrolled magnetizing inductance (dashed). In region *a* control is completely lost, see Fig. 8.

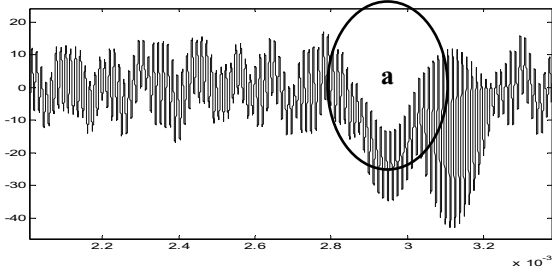


Fig. 8. In addition to Fig. 7, the output current ($i_{res} - i_m$) in region *a* does not cross zero anymore.

Fig. 8 shows the computer simulated consequence of the DC-component of the magnetizing current being larger than the resonant current amplitude. The output current does not cross zero anymore, therefore the switches stay in the same state and control is lost for some time.

This can be avoided by ensuring a negative integral in (9) after a positive integral (and vice versa) in the previous quantum period, which balances out the DC component in the current. To achieve this, after a change in controller input u ($1 \rightarrow -1$, or $-1 \rightarrow 1$), u is set to 0 (free-resonance) for only the next quantum. Assuming proper resonant operation, the sign term in (9) changes polarity each quantum and therefore the integral changes sign each quantum as required. If now a change in u occurs, two consecutive positive (or negative) integrals will follow unless u is set to 0.

As a result, the magnetizing current is bounded by (10).

$$|i_m| < \frac{V_{ref}}{4L_m f_{res}} \quad (10)$$

If $4L_m f_{res} > R_{load}$, the system will be stable for the same reference current I_{ref} as without magnetizing inductance. Otherwise, an additional current penalty is required to obtain a stable closed-loop system.

Fig. 9 shows an example of a situation where the magnetizing current amplitude is almost half the resonant

current amplitude. The system is stable, even despite a phase shift of one fifth of a quantum period.

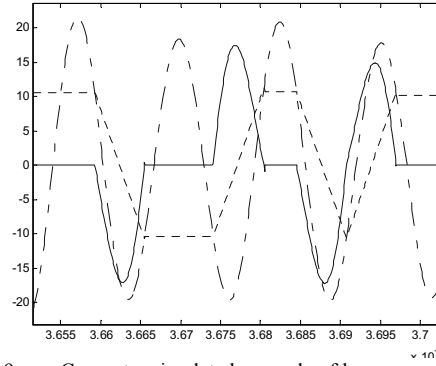


Fig. 9. Computer simulated example of large magnetizing current (dotted) compared to the resonant current (dash-dot). Also shown is the output current (solid).

F. Controller layout

To conclude this chapter, the quantum controller for the input converter is simply first order. The effective amplitude of the measured current, approximated by low-pass filtering the absolute resonant signal, is compared to the reference current. For better performance with less scattering, hysteresis or higher order control is possible.

The switches change state at the zero-crossing of the current through the present conducting switches, which is represented by the synchronization block in Fig. 10.

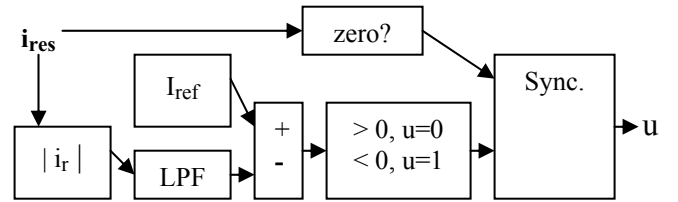


Fig. 10. Functional diagram of input controller

The output control in Fig. 11 is the same, except that the filter is absent because the low-frequency output voltage already is nearly constant during a switching cycle. Also, the synchronization is a little more complicated to implement the switching strategy of Fig. 6, as introduced in section E.

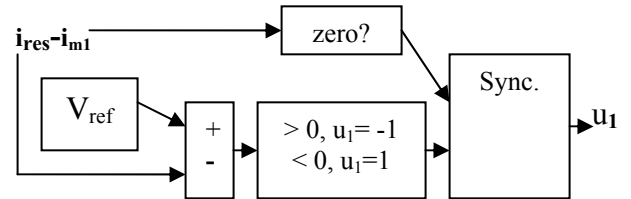


Fig. 11. Functional diagram of output controller

IV. EFFICIENCY

Limitation of the previous strategy is the fact that the resonant current amplitude is fixed at the minimum required level for stable operation in the worst case situation. In this

‘worst case’ the system efficiency will be maximal, because a minimum current is reflected back to the source. Though, in the remainder of the operating region the efficiency is suboptimal. Solution probably is to introduce a time-dependent reference for the current. The latter step has not been done, because a proof of principle in practice with fixed reference was considered of primary importance.

V. CONTROLLER IMPLEMENTATION

Each of the controllers consists of an analogue part in combination with a digital part. The digital part was chosen a TMS320f2808 DSP from Texas Instruments. All controller functions could be implemented also with only analogue circuitry, but for testing purpose a DSP is more flexible.

On the other hand, using a DSP without analogue pre-processing parts until now is not an option at 100 kHz, because the on-chip peripherals (e.g. analogue/digital inputs and outputs) are currently the limiting factor in processing speed.

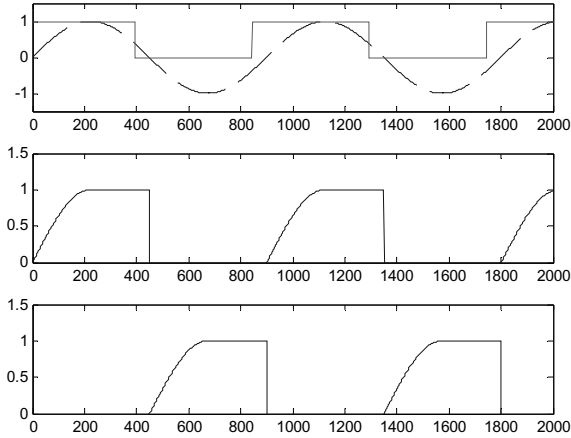


Fig. 12. Analogue output signals, with a) zero-crossing detection (block signal) before actual crossing of the sinus, b) maximum-hold of positive part of the sinus and c) maximum-hold of negative part of the sinus.

For the analogue part, the maximum of the resonant current in every quantum period is hold to make it available for the DSP for some time, which relieves the digital timing. Also, the positive and negative parts are split in two separate signals to keep track of the resonant current polarity.

Most important analogue function is to detect the zero-crossing of the current. To account for processing time of the drivers and digital part the crossing must be detected earlier than the actual crossing. To obtain such predictive detection two methods were considered.

The first is to use amplitude variable (inverted) hysteresis as shown in Fig. 13. Here, the current is compared with a variable amplitude block signal. The instantaneous amplitude of the block depends on the amplitude of the previous current quantum, to ensure an approximate constant anticipation time, which is independent of the current amplitude.

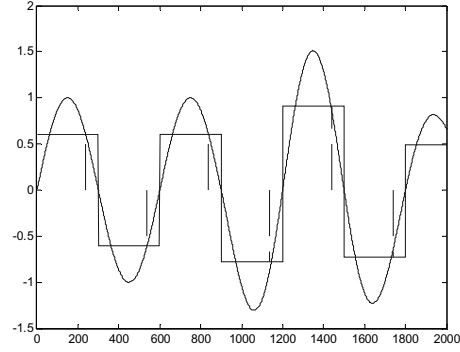


Fig. 13. Predictive zero-current detection. The dashed lines project the intersections between block signal and sinusoidal signal on the time-axis. The amplitude of the block signal is variable and depends on the amplitude of the previous current quantum. Only intersections with the block signal after a maximum in the current are detected as zero-crossing.

The second method, which is implemented in the prototype, uses the principle of an input driven harmonic oscillator. The oscillator consists of a parallel RLC circuit as in Fig. 14.

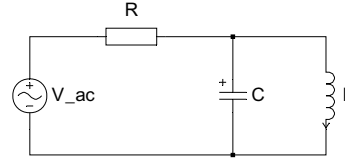


Fig. 14. Electrical circuit for harmonic oscillator zero-current detection.

The circuit is driven by a sinusoidal source, which in case of the prototype is a voltage, representing the measured resonant current. Equation (11) states the circuit in terms of inductor current i_L for a normalized sinusoidal source.

$$RCL \frac{d^2 i_L}{dt} + L \frac{di_L}{dt} + Ri_L = \cos(\omega t) \quad (11)$$

A solution for the second order differential equation is given in (12).

$$i_L(t) = \frac{1}{Z\omega} \sin(\omega t - \alpha) \quad (12)$$

where

$$Z = \sqrt{L^2 + \left(\omega RCL - \frac{R}{\omega} \right)^2}, \quad \alpha = \arctan \left(\frac{\omega RCL - \frac{R}{\omega}}{L} \right)$$

With (12), also the voltage across the capacitor (and inductor) is known, see (13).

$$u_C(t) = u_L(t) = \frac{L}{Z} \cos(\omega t - \alpha) \quad (13)$$

From this, it is clear that by choosing C and L an arbitrary phase change can be realized between driving and output-capacitor voltage. The absolute current amplitude is not of importance for zero-crossing detection. Besides realizing a phase shift, the oscillator behaves like a band-pass filter. The

filtering property is important, because the phase-shifted signal is fed to a differential amplifier and is therefore sensitive to noise. It is assumed that the resonant frequency of the main cable does not change significantly by removing and adding a clamp, thus the method works with fixed R, L and C of the oscillator. If necessary, the R and therefore also the phase can be adjusted during operation the same as in the first method.

VI. EXPERIMENTAL RESULTS

The reference output voltage has been chosen triangular for simplicity. This reference is software generated and consists of a timer running up and down linearly. For sinusoidal output a table with sinusoidal entries should be required. Because the computer timer ran at 100 MHz and division is possible at exact powers of 2, result most close to 60 Hz was an output triangular voltage of 80 Hz as shown in Fig. 15 for a single clamp. Corresponding resonant current and voltage across the resonant capacitor are shown in Fig. 16.

Figs. 15 and 16 denote a low-power experiment, which is a safety measure against the effect of disturbances that might destroy some parts of the experimental setup. The current layout of the setup is quite open for measurements and therefore also sensitive to noise.

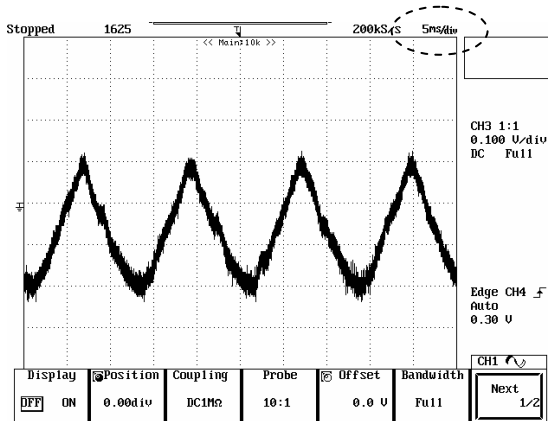


Fig. 15. Triangular output voltage of single clamp. Note that 4 periods in 50 ns gives a frequency of 80 Hz. The waveform has been measured with a 1:20 voltage meter, therefore the peak voltage as shown here is 30 V.

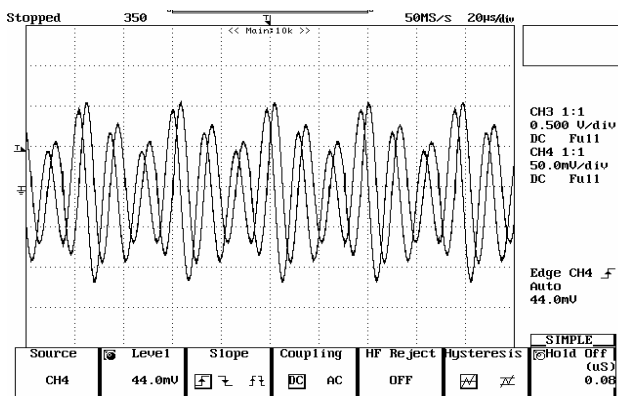


Fig. 16. Prototype snapshot of current amplitude control. Also shown is the voltage (the largest in amplitude of the two) across the resonant capacitor.

Table II lists parameter values for the system corresponding to the experimental waveforms in Figs. 15 and 16.

TABLE II
PARAMETER VALUES FOR THE CABLE WITH CLAMPS REFERRING TO FIG. 15
AND FIG. 16

Symbol	Quantity	Value
V_{in}	Input voltage	10 [V]
C_f	Filter capacitor	10 [μF]
$R_{1,2}$	Load resistances	200 [Ω]
I_{ref}	Reference resonant current amplitude	0.7 [A]

VII. CONCLUSION

An experimental proof of principle has been given for a contactless system with triangular 80 Hz output voltage waveforms for multiple (two) loads. The blinded input and output controllers were implemented on a multiple sliding-surface quantum conversion theory basis. This stable basis with a time-independent reference current should be extended to a time-dependent reference to obtain an improved efficiency. To deal with the relative small magnetizing inductances of the cable-clamp magnetic connections standard quantum conversion strategy has been extended with a method to limit the magnetizing current.

REFERENCES

- [1] J. W. Jansen, C. M. M. Van Lierop, E. A. Lomonova, A. J. A. Vandeput, "Modeling of Magnetically Levitated Planar Actuators With Moving Magnets", IEEE Transactions on Magnetics, Vol. 43, No. 1, January 2007
- [2] S. Y. R. Hui, W. W. C. Ho, "A new generation of universal contactless battery charging platform for portable consumer electronic equipment", IEEE Transactions on Power Electronics, Vol. 20, Issue 3, May 2005, pp. 620-627
- [3] F. F. A. Van der Pijl, J. A. Ferreira, P. Bauer, H. Polinder, "Design of an Inductive Contactless Power System for Multiple Users", Conference Record of the 2006 IEEE 41st IAS Annual Meeting, Vol. 4, pp. 1876-1883, October 2006
- [4] G. B. Joung, J. G. Cho, G. H. Cho, "A Generalized Quantum Resonant Converter Using a New Quantumresonant Module", IEEE Transactions on Power Electronics, Vol. 7, Issue 4, October 1992
- [5] M. Castilla, L. Garcia de Vicuña, M. Lopez, O. Lopez, J. Matas, "On the Design of Sliding Mode Control Schemes for Quantum Resonant Converters", IEEE Transactions on Power Electronics, Vol. 15, Issue 6, November 2006
- [6] M. Castilla, L. Garcia de Vicuña, J. Ordinas, "Modeling and Multi-Input Sliding Mode Control of the Series Resonant Converter", Proceedings of the 1998 Power Electronics Motion Control Conference, pp. 5/105-5/110
- [7] M. Castilla, L. Garcia de Vicuña, J. M. Guerrero, J. Matas, J. Miret, "Sliding-Mode Control of Quantum Series-Parallel Resonant Converters Via Input-Output Linearization", IEEE Transactions on Industrial Electronics, Vol. 52, Issue 2, pp. 566-575, April 2005
- [8] V. I. Utkin, Sliding Modes in Control Optimization, Springer-Verlag, 1992
- [9] S. R. Sanders, J. M. Noworolski, X. Z. Liu, G. C. Verghese, "Generalized Averaging Method for Power Conversion Circuits", IEEE Transactions on Power Electronics, Vol. 6, Issue 2, pp. 251-259, April 1991
- [10] J. J. Slotine, W. Li, Applied Nonlinear Control, Prentice-Hall, 1991